Beam Steering in Narrow-Stripe High-Power 980-nm Laser Diodes

W. D. Herzog, B. B. Goldberg, and M. S. Ünlü

***Abstract*—We used near-field scanning optical microscopy to measure the optical beam characteristics of weakly-guided narrow-stripe high-power laser diodes. For both facets of the device, we correlate changes in the near-field optical characteristics with beam steering and the kink in the light output versus operating current curve. Our measurements demonstrate that: 1) frequency-locking of lateral modes exists for operating currents below the kink in the L–I curve; 2) beam steering is a result of a shift of in the beat-length pattern inside the laser cavity of the frequency-locked lateral modes; and 3) the kink in the L–I curve results from a sudden increase in the beam waist of the guided-modes.**

***Index Terms*—Beam steering, fiber amplifiers, optical waveguides, semiconductor lasers, semiconductor waveguides.**

HIGH-POWER 980-nm laser diodes are currently used to optically pump erbium-doped fiber amplifiers for telecommunication systems. In this capacity, the laser diode must reliably provide high output power in a stable optical beam with efficient power coupling to the waveguide mode of the fiber amplifier. To this end, narrow-stripe devices capable of single spatial mode operation are utilized. These devices typically employ weak lateral guiding to ensure single-mode operation while maximizing the spatial size of the fundamental mode to reduce the peak power density and, thus, prevent catastrphic optical damage (COD) on the output facet [1]. In this letter, near-field scanning optical microscopy (NSOM) is used to image the output of a 980-nm graded-index separate-confinement heterostructure (GRINSCH) laser diode, which exhibits a kink in the light versus current (L–I) curve and lateral beam-steering. Measurements were performed on the output of both the antireflection (AR) and high-reflection (HR) coated facets. We correlate the NSOM images of the laser near field with far-field measurements of beam-steering as a function of the laser diode operating current with an emphasis on the behavior at around the L–I kink.

The NSOM technique utilizes a subwavelength aperture, scanned in the near-field to generate an optical image [2], [3]. Critical to the implementation of NSOM is the fabrication of high-quality optical probes and a height regulation system to maintain a controlled proximity of the NSOM probe to the sample. Two varieties of optical probes were used for this work. For the HR facet, the traditional heat-and-pull tapered metal-coated optical fiber NSOM probe was used [4]. For the AR facet, the enormous power density of the laser prohibited the use of metal-coated NSOM probes and necessitated the use of uncoated probes. Although the spatial resolution of uncoated probes is $\sim$1 μm and significantly inferior to that of metal-coated probes, it is still much smaller than the lateral mode diameter of the laser. Detailed studies of uncoated probes found that they were sufficient for accurate imaging of the lateral mode of the GRINSCH laser diode [5]. Height regulation was accomplished by shear-force detection provided by the tuning-fork method [6]. Simultaneous collection of optical images and surface topography allowed the laser output to be correlated with the device structure.

The GRINSCH laser diode in this work is rated to provide 200 mW of kink-free power. The device is 750 μm long and has 10% and 90% reflectances for the AR and HR facets, respectively. A narrow-ridge $\sim$3 μm in width at its top and $\sim$4.5 μm at its base, provides lateral index-guiding. Similar to previous reports, beam steering was only observed for current pulses longer than $\sim$1 μs [7]. In order to balance the needs of minimizing power on the NSOM probe to prevent probe failure, and pulse lengths sufficiently long to generate the quasi-continuous wave (CW) beam-steering phenomenon, 10-μs pulses were applied to the device at a 1% duty cycle for all of the measurements.

Fig. 1 shows NSOM images of the laser mode on the device facet. The scan size for each image is 5×10 μm. Superimposed on the gray-scale image of the surface topography are equi-intensity contours of the laser output. Fig. 1(a)–(c) was collected on the AR facet of the device while Fig. 1(d)–(f) was obtained on the HR facet at three different operating currents selected based on the far-field beam pointing behavior of the laser diode. Beam pointing measured on both laser facets is shown in Fig. 2 displaying a maximum beam steering at an operating current of $I \sim 220$ mA. The onset of beam steering is consistent with the kink in the L–I curve measured in the far field. To verify that the same L–I characteristics exist in the near field of the laser diode, we measured the total power emitted by integrating the NSOM image on the AR facet of the GRINSCH laser diode [as in Fig. 1(a)–(c)] and plot the integrated intensity as a function of operating current (see the inset to Fig. 2). Equivalent to far-field L–I measurements, the NSOM data displays a kink in the L–I curve at $I = I_k \sim 200$ mA.

A closer inspection of the NSOM images (Fig. 1) in the vicinity of the current level corresponding to the kink in the L–I curve shows dramatic variations. For an operating current of $I = (100 \text{ mA}) < I_k$, Fig. 1(a) shows that the laser output is laterally shifted on the AR facet relative to the mesa. Meanwhile, Fig. 1(d) shows that the laser output is centered on

Manuscript received July 31, 2000. This research was supported in part by NSF CAREER Grant ECS 3625236, NSF ARI Grant 9413855, and ARO Grant DAAG-55-98-1-0143.

The authors are with the Department of Electrical and Computer Engineering, Department of Physics, Photonics Center, Boston University, Boston, MA 02215 USA (e-mail: selim@bu.edu).

Publisher Item Identifier S 1041-1135(00)10609-3.

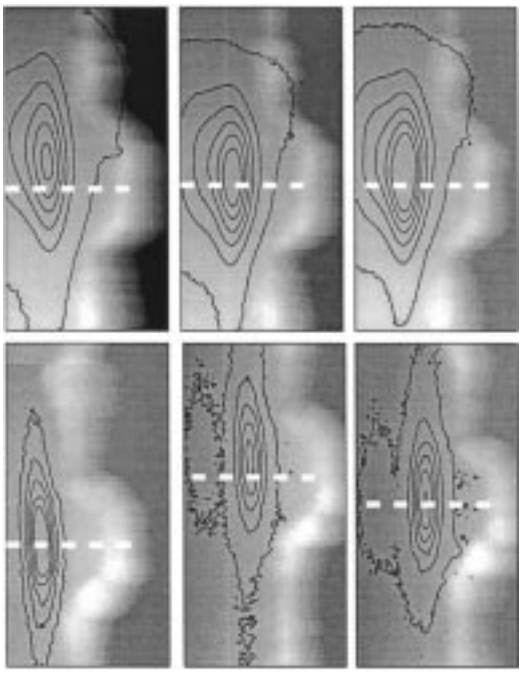

Fig. 1. NSOM images of the GRINSCH laser diode. Superimposed on the gray-scale images of the surface topography are equi-intensity contours of the optical output of the laser. White dashed lines have been added as a guide; (a)–(c) were collected on the AR facet for $I = 100$ mA, $I = 220$ mA and $I = 240$ mA, respectively; (d)–(f) were collected on the HR facet for the same set of operating currents.

the HR facet for the same operating current. When maximum beam steering is observed in the far field $I \sim 220$ mA, the laser output shifts toward the center of the mesa for the AR facet [Fig. 1(b)], while the mode is offset toward the edge of the mesa for the HR side of the device [Fig. 1(e)]. Finally, for $I = 240\ \text{mA} \gg I_k$, Fig. 1(c) and (f) display that the laser output returns toward its original position on both facets. The bottom panel in Fig. 3 summarizes the lateral shift of the laser output on the device facets relative to the center of the mesa as a function of operating current. Fig. 3 also shows the lateral beam waists measured in the near field, revealing a sudden increase at the current corresponding to L–I kink.

We discuss the lateral optical field in terms of Hermite–Gaussian modes. While the Hermite–Gaussian modes are only an approximation to the actual waveguide solution, they serve to give an intuitive understanding of the data. In terms of the beam waist w and the beam waist minimum w_0, the equation for a Hermite–Gaussian field, $U(\vec{r})$, propagating in the z-direction, is given by

$$U(\vec{r}) = A_{l,m}\left[\frac{w_0}{w(z)}\right] G_l\left[\frac{\sqrt{2}x}{w(z)}\right] G_m\left[\frac{\sqrt{2}y}{w(z)}\right] \times \exp\left[+ikz + ik\frac{x^2+y^2}{2R(z)} - i(l+m+1)\zeta(z)\right] \tag{1}$$

$$R(z) = z\left[1+\left(\frac{z_0}{z}\right)^2\right]; \quad \zeta(z) = \tan^{-1}\left(\frac{z}{z_0}\right).$$

In our analysis, the transverse dimension of the laser structure is described by the fundamental field profile $G_{m=0}$, while the

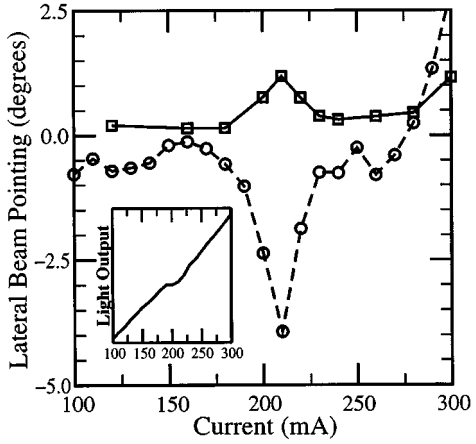

Fig. 2. Inset shows the light output versus operating current collected through the NSOM probe on the AR facet. The main figure shows the far-field beam pointing versus operating current for the AR facet (circles) and HR facet (squares). The data are slightly offset from zero pointing angle for clarity.

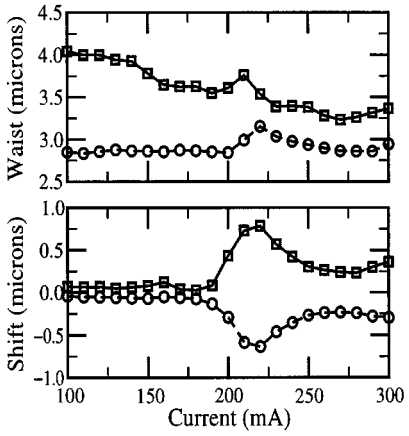

Fig. 3. (a) Lateral beam waists at the AR facet (circles) and HR facet (squares) as a function of operating current. (b) Lateral peak position of the near-field intensity versus operating current obtained with NSOM for the AR facet (circles) and HR facet (squares). The data sets are slightly offset from zero for clarity.

first two lateral profiles $G_{2=0,1}$ are necessary to describe the lateral-mode behavior. Two important phenomena resulting from coherent superposition of two lateral modes are spatial beat-length patterns along the length of the laser cavity and beam steering of the far-field emission. The beating patterns were previously observed in spontaneous emission imaged through the laser substrate and were also inferred from a periodic dependence of beam-steering direction on cavity length [8], [9]. The beat-length pattern results from the difference in propagation constants of the first two lateral modes, resulting in a monotonically varying phase between the two fields as a function of position along the laser cavity. Coherent mode superposition also explains beam steering, which results from the term $\zeta(z)$. In the near field $\zeta(z) = 0$, while in the far-field, $\zeta(z) = \pi/2$. The factor $(l+m+1) \times \zeta(z)$ results in an accumulated phase difference between the two modes of the field as it propagates from the near field to the far field. In this way, a beam that is centered in the near field with a phase difference between the modes of $\pm\pi/2$ is shifted in the far field with a phase difference of zero or π.

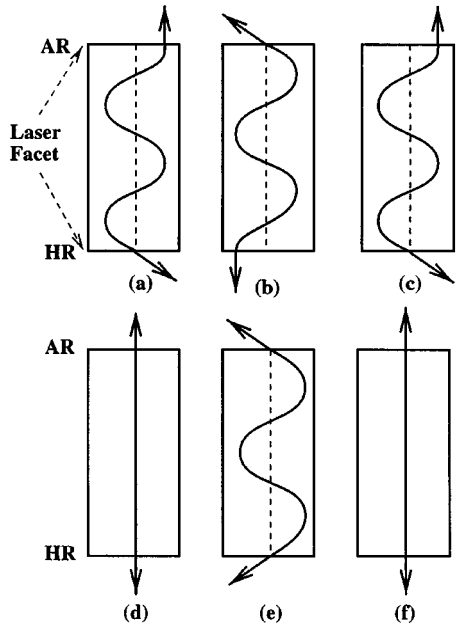

Fig. 4. Schematic representations of the lateral peak intensity position of the guided mode(s) along the length of the laser cavity. The top series of figures are used to explain our NSOM and far-field data. (a) Coherent propagation of the first two lateral modes for $I < I_k$. The peak intensity shifts from side to side due to the difference in propagation constants of the two lateral modes. The difference in phase accumulation along the propagation direction results in a beat-length pattern. (b) Shift in the beat-length pattern inside the laser cavity for $I \sim I_k$. Note that the beat length did not change. (c) Return of the beat-length pattern to its former state for $I \gg I_k$. The bottom series of figures depict previous interpretations of beam-steering. (d) Single-mode laser operation for $I < I_k$. (e) Coherent propagation of the first two lateral modes for $I \sim I_k$. (f) Incoherent propagation of multiple modes for $I \gg I_k$.

Our interpretation of beam pointing based on the near-field and far-field measurements predicts two lateral modes frequency locked for all operating currents resulting in a total intensity staggering side to side along the cavity. The solid lines in Fig. 4 schematically represents the lateral position of the peak intensity along the length of the laser cavity. The position of the resulting lateral-mode pattern is a function of the relative phase difference between the two modes. The coherent superposition of these modes results in a spatially centered beam on the HR facet and a laterally shifted beam on the AR facet for $I = 100$ mA $< I_k$ as seen in Fig. 4(a). Beam steering occurs when the beat-length pattern shifts inside the cavity by 1/4 of the beat length, shown in Fig. 4(b). When $I \gg I_k$, the beat-length pattern returns to its former state. This interpretation differs significantly from previous interpretations of beam steering in which the laser is described as operating with a single mode for $I < I_k$ [8]–[10]. Schematically, the previous interpretation is depicted in Fig. 4(d)–(f). The kink in the L–I curve then occurs at the lasing threshold for the second lateral mode. Eventually, as the current in increased above the kink in the L–I curve, frequency-locking occurs and coherent superposition of the modes generates beam steering. Finally, for $I \gg I_k$, locking breaks and two incoherent modes propagate along the axis of the laser cavity.

The interpretation of beam steering put forth in this letter is necessary to explain both the near-field and far-field data. Furthermore, by our interpretation, the change in the propagation direction of the far-field beam mirrors that of the previous theory. Also, the kink in the L–I curve is explained by the NSOM data. As shown in the top panel of Fig. 3, the near-field lateral beam waist for both facets display a sudden increase at the kink current I_k. Due to increase of the beam size, a decrease in the spatial overlap of the optical intensity with the gain region results in a decrease in lasing efficiency. Hence, a kink in the L–I curve is observed.

With the use of NSOM, we have imaged the near field of a 980-nm high-power laser diode and analyzed beam steering at operating current corresponding to a kink in the L–I curve. Our results indicate that shifting of the beat-length pattern inside the semiconductor cavity is responsible for the change in angular emission associated with narrow-stripe beam-steering lasers. We also observe that the beam is off-center toward one side of the mesa on the AR-coated output facet at currents $I < I_k$ and after moving toward the center at the kink it returns to approximately the same position for higher currents. Considering that for a symmetrical structure beam position on either side of the mesa should be equally probable, we speculate that a stable position for the off-center beam is determined by a subtle asymmetry in the device. Therefore, for a actively aligned fiber coupling system where the fiber position is not aligned to the physical structure but adjusted to maximize the coupled light, coupling efficiency at currents above the kink may not be significantly affected.

REFERENCES

[1] J. Näppi, A. Ovtchinnikov, H. Asonen, P. Savolainen, and M. Pessa, "Limitations of two-dimensional passive waveguide model for $\lambda = 980$ nm Al-free ridge waveguide lasers," *Appl. Phys. Lett.*, vol. 64, p. 2203, 1994.

[2] B. B. Goldberg, M. S. Ünlü, W. D. Herzog, and E. Towe, "Near-field optical microscopy and spectroscopy of heterostructures and laser diodes," *IEEE J. Select. Topics Quantum Electron.*, vol. 1, pp. 1073–1081, Dec. 1995.

[3] D. W. Pohl, W. Denk, and M. Lanz, "Optical stethoscopy—Image recording with resolution $\lambda/20$," *Appl. Phys. Lett.*, vol. 44, p. 651, 1984.

[4] E. Betzig, A. Lewis, A. Harootunian, M. Isaacson, and E. Kratshmer, "Near-field scanning optical microscopy (NSOM)—Development and biophysical applications," *Biophys. J.*, vol. 49, p. 268, 1986.

[5] W. D. Herzog, "Near-field scanning optical microscopy of semiconductor lasers and materials," Ph. D. dissertation, Boston Univ., Boston, MA, 2000.

[6] K. Karrai and R. D. Grober, "Piezoelectric tip-sample distance control for near field optical microscopes," *Appl. Phys. Lett.*, vol. 66, pp. 1842–1844, 1995.

[7] G. Hunziker and C. Harder, "Beam quality of InGaAs ridge lasers at high-output power," *Appl. Opt.*, vol. 34, pp. 6118–6122, 1995.

[8] J. Guthrie, G. L. Tan, M. Ohkubo, T. Fukushima, Y. Ikegami, T. Ijichi, M. Irikawa, R. S. Mand, and J. M. Xu, "Beam instability in 980-nm power lasers: Experiment and analysis," *IEEE Photon. Technol. Lett.*, vol. 6, pp. 1409–1411, Dec. 1994.

[9] M. F. C. Schemmann, C. J. van der Poel, B. A. H. van Bakel, H. P. M. M. Ambrosius, A. Valster, J. A. M. van den Heijkant, and G. A. Acket, "Kink power in weakly index guided semiconductor lasers," *Appl. Phys. Lett.*, vol. 66(8), pp. 920–922, 1995.

[10] G. Tan, R. S. Mand, and J. M. Xu, "Self-consistent modeling of beam instabilities in 980-nm fiber pump lasers," *IEEE J. Quantum Electron.*, vol. 33, pp. 1384–1395, Aug. 1997.